Multifunctional Hybrid Structure of SVC and Capacitive Grid-Connected Inverter (SVC//CGCI) for Active Power Injection and Nonactive Power Compensation

Lei Wang, *Member, IEEE*, Chi-Seng Lam, *Senior Member, IEEE*, and Man-Chung Wong, *Senior Member, IEEE*

***Abstract*—In this paper, the structure, coordinate control method, and parameter design of a hybrid system are proposed for active power injection and nonactive power (reactive, harmonic, and unbalance power) compensation. The proposed hybrid system consists of a static var compensator (SVC) in parallel with a capacitive-coupling grid-connected inverter (CGCI) (SVC//CGCI). In SVC//CGCI, the SVC part is used to dynamic compensate the reactive power and unbalance power, while the low rating CGCI part is used to inject active power, provide harmonic power and a fixed amount of capacitive reactive power. Compared with conventional inductive-coupling grid-connected inverter (IGCI), the CGCI can provide active, reactive and harmonic power with low rating of active inverter part. The cost of the SVC part is much lower than that of active inverter part, thus the reduction of inverter rating can lead to a decrease in the total cost of the SVC//CGCI. Therefore, the SVC//CGCI can be a cost effective solution for active power injection and nonactive power compensation. Finally, simulation and experimental results are provided to show the advantages and validity of the proposed SVC//CGCI in compared with the conventional IGCI and SVC//IGCI.**

***Index Terms*—Active power injection, capacitive grid connected inverter (CGCI), harmonic current compensation, inductive coupling grid connected inverter (IGCI), reactive power compensation, static var compensator (SVC).**

Manuscript received July 9, 2017; revised January 8, 2018 and March 20, 2018; accepted May 2, 2018. Date of publication May 24, 2018; date of current version October 31, 2018. This work was supported in part by the Science and Technology Development Fund, Macao SAR (FDCT) under Grant 025/2017/A1 and Grant 109/2013/A3 and in part by the Research Committee of the University of Macau under Grant MYGR2017-00038-FST and Grant MYRG2017-00090-AMSV. *(Corresponding author: Chi-Seng Lam.)*

L. Wang is with the Department of Electrical and Computer Engineering, Faculty of Science and Technology, University of Macau, Macau 999078, China.

C.-S. Lam is with the State Key Laboratory of Analog and Mixed Signal VLSI, University of Macau, Macau 999078, China (e-mail: c.s.lam@ieee.org; cslam@umac.mo).

M.-C. Wong is with the Department of Electrical and Computer Engineering, Faculty of Science and Technology and also with the State Key Laboratory of Analog and Mixed Signal VLSI, University of Macau, Macau 999078, China.

Color versions of one or more of the figures in this paper are available online at http://ieeexplore.ieee.org.

Digital Object Identifier 10.1109/TIE.2018.2838085

I. Introduction

THE grid is the interconnection of different power systems, from high-voltage transmission systems to low-voltage distribution systems, from centralized generation to distributed generation, from utility control centers to end-user home-area networks, and from traditional energy resources to renewable generation energy resources [1]. However, the development of the smart grid brings many new challenges on power quality [2], especially in weak grid area the small power quality problem can lead to severe consequence. Therefore, the multifunctional grid-connected inverters have been paid more and more attentions for their benefits on power quality improvement and renewable power integration.

Traditionally, the task of inductive grid-connected inverters (IGCIs) is used to transfer active power from renewable energy resources to the power grid. However, the integration of uncontrollable resources, such as wind and solar energy, can also cause power quality problems to the grid. Therefore, apart from renewable integration function, many researchers suggest to embed the power quality enhancement function in the IGCIs. As the active power flow is orthogonal to the reactive power flow, it is economical to use the same inverter to transfer active and reactive power simultaneously. To attach reactive power and active power transfer, the different control strategies have been proposed for IGCIs [3]–[8]. However, the harmonic and unbalanced power compensation abilities have not been included in the above control methods [3]–[8]. To include reactive, harmonic and unbalanced compensation abilities, the more general control strategies have been proposed in [9]–[12], etc.

According to the cost study in [13]–[15], the cost of the IGCI or active power filter (APF) is about \$60/kVA and the costs of static var compensator (SVC) and passive power filter (PPF) are about \$18/kVA and \$5/kVA. From the cost reduction point of view, as the costs of the SVC and PPF are much lower than that of active inverter part, the reduction of active inverter part capacity can lead to a decrease in the total cost of hybrid topologies. The different hybrid systems have been reported in literatures, such as passive power filter in parallel with APF (PPF//APF) [16], [17], SVC in parallel with APF (SVC//APF) [18], SVC in parallel with static synchronous compensator (SVC//STATCOM) [19], SVC in series with hybrid SPF (SVC-HAPF) [20]–[24], SVC in parallel with HAPF (SVC//HAPF) [25], etc. In this paper, a new hybrid system: SVC in parallel with CGCI (SVC//CGCI) is proposed. Compared with [16]–[24], the proposed SVC//CGCI has lower inverter's voltage rating than the PPF//APF, SVC//APF, SVC//STATCOM, and lower inverter's current rating than the SVC-HAPF. Moreover, the proposed SVC//CGCI has considered the active power injection, which is not included in [16]–[25]. The contributions of the proposed SVC//CGCI can be listed from different points of view.

1) From the characteristic point of view, the proposed SVC//CGCI combines the advantages of both SVC [26]–[28] and CGCI [29], [30], which address the inherent problems of them.
2) From the functionality point of view, the proposed SVC//CGCI can be used for both active power injection and nonactive power dynamic compensation simultaneously. However, both SVC and CGCI cannot obtain the aforementioned functions when using alone.
3) From the parameter design point of view, the proposed parameter design method includes the considerations of reactive power sharing between SVC//CGCI, active power injection and the harmonic currents rejection.
4) From the control point of view, the unique coordinate control of the SVC part and CGCI part is proposed to coordinate the SVC part and the CGCI part for active power injection and nonactive power.

In the following Section II, the circuit configuration of the three-phase three-wire SVC//CGCI are presented. Based on the circuit configuration, the operation principle and coordinated control between SVC and CGCI are proposed in Section III. Then, the parameter design method of the SVC//CGCI is given in Section IV. After that, to show the advantages of the proposed SVC//CGCI, the simulation comparisons of the IGCI, SVC//IGCI, and the proposed SVC//CGCI are provided in Section V. In Section VI, representative experimental results are given based on laboratory-scaled hardware prototype. Finally, conclusion will be drawn in Section VII.

II. Circuit Configuration of the Three-Phase SVC//CGCI

Fig. 1 shows the system topology of a three-phase three-wire SVC//CGCI. In this paper, the subscript "x" denotes phase $x = a, b, c$; v_{sx}, v_x, and $v_{\mathrm{inv}x}$ are the source voltage, load voltage, and inverter voltage, respectively. i_{sx}, i_{Lx}, and i_{cx} are source current, load current, and compensating current, respectively. The SVC part of the SVC//CGCI consists of a coupling inductor L_c, a parallel capacitive C_{PF} and a thyristor-controlled reactor with an inductor L_{PF}.The CGCI part consists of coupling LC filter (L_p and C_p), a two-level voltage source inverter (VSI) and a dc-link capacitor C_{DC}. The CGCI part has both low-voltage rating due to large voltage drop on LC and low-current rating due to the current divider between i_{cx1} and i_{cx2}.

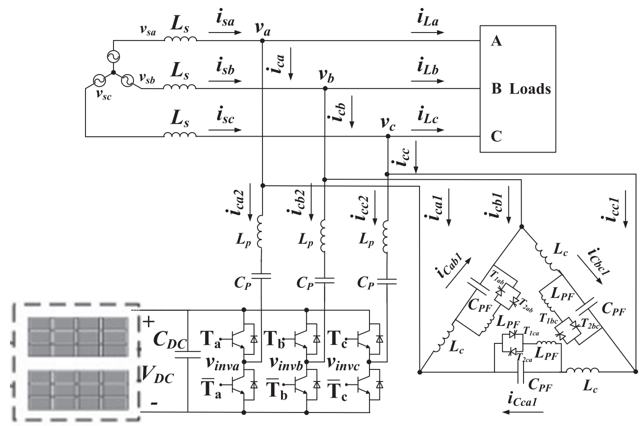

Fig. 1. Circuit configurations of the SVC//CGCI.

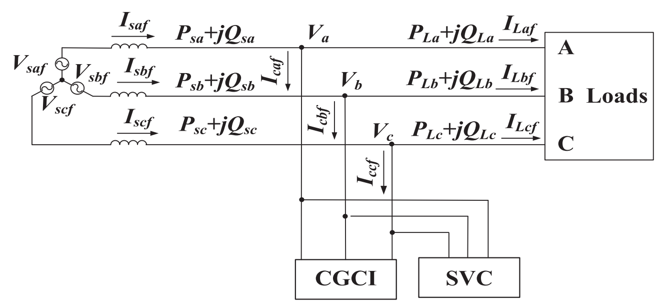

Fig. 2. Power flow analysis for unbalanced power compensation.

III. Operation Principle and Coordinated Control of SVC//CGCI

In this section, the operation principle and coordinated control of SVC//CGCI are discussed and explained into the following three parts.

1) *Part A*: SVC part control.
2) *Part B:* CGCI part control.
3) *Part C:* The overall control block.

A. Operation Principle and Control of the SVC Part

The SVC part of SVC//CGCI is used to dynamically compensate the fundamental load unbalanced and reactive power by controlling its firing angles. The key concept of the SVC part control can be described in Section III-A1. The controls of the SVC part in delta connection are explained in Section III-A2.

1) Operation Principle and Concept of SVC Part: In this paper, the study of the proposed SVC//CGCI is based on balanced three-phase source voltage assumption. For the three-phase three-wire system, the unbalanced source active power can be automatically controlled to be balanced when the unbalanced reactive power is compensated to be balanced [24], [26]. Fig. 2 shows the power flow analysis of SVC//CGCI compensation.

The phase fundamental source apparent power is defined as: $S_{sx} = P_{sx} + jQ_{sx} = \overrightarrow{V}_{sx} \cdot \overrightarrow{I}^*_{sxf}$, where the note "*" denotes the complex conjugate. In Fig. 2, the sum of $\vec{I}^*_{sxf}$ can be expressed as [26]

$$\vec{I}^{*}_{saf}+\vec{I}^{*}_{sbf}+\vec{I}^{*}_{scf}=\frac{P_{sa}+jQ_{sa}}{\vec{V}_{saf}}+\frac{P_{sb}+jQ_{sb}}{\vec{V}_{sbf}}+\frac{P_{sc}+jQ_{sc}}{\vec{V}_{scf}}=0 \quad (1)$$

where $\vec{I}_{saf}$, $\vec{I}_{sbf}$, and $\vec{I}_{scf}$ are the fundamental source current phasors. $\vec{V}_{saf}$, $\vec{V}_{sbf}$, and $\vec{V}_{scf}$ are the fundamental source voltage phasors. $\vec{V}_{saf}$ is set to be the reference phasor, so $\vec{V}_{saf}=\bar{V}_{sxf}\angle 0^{o}$, $\vec{V}_{sbf}=\bar{V}_{sxf}\angle-120^{o}$, and $\vec{V}_{scf}=\bar{V}_{sxf}\angle 120^{o}$, where $1\angle-120^{o}=-1/2-j\sqrt{3}/2$ and $1\angle 120^{o}=-1/2+j\sqrt{3}/2$, V_{sxf} is the root-mean-square (RMS) value of the source voltage. Simplifying (1), one can get

$$\left(2P_{sa}-P_{sb}-\sqrt{3}Q_{sb}-P_{sc}+\sqrt{3}Q_{sc}\right)+j\left(2Q_{sa}-Q_{sb}+\sqrt{3}P_{sb}-Q_{sc}-\sqrt{3}P_{sc}\right)=0 \quad (2)$$

In (2), both real part and imaginary part are equal to zero. Thus, the following relationship can be obtained as

$$\begin{aligned}&2P_{sa}-P_{sb}-\sqrt{3}Q_{sb}-P_{sc}+\sqrt{3}Q_{sc}=0\\&2Q_{sa}-Q_{sb}+\sqrt{3}P_{sb}-Q_{sc}-\sqrt{3}P_{sc}=0.\end{aligned} \quad (3)$$

If the source reactive power is compensated to be balanced by SVC part as (4), the source active power can be balanced as (5).

$$Q_{sa}=Q_{sb}=Q_{sc}=Q_{LC} \quad (4)$$

where Q_{sx} is source reactive power, Q_{LC} is the fixed value which is provided by the coupling LC of CGCI part. By substituting (4) into (3), the relationship of the three-phase source active power can be obtained as

$$P_{sa}=P_{sb}=P_{sc}. \quad (5)$$

Based on the analysis of (1)–(5), it can be concluded that the source active power can become balanced once the reactive power is compensated to be balanced.

2) SVC Part Control: The purpose of this part is to obtain the firing angle (α_{xy}) of the SVC part to compensate the phase source reactive power Q_{sx} to equal Q_{LC}, so that the left small Q_{LC} can be compensated by CGCI. Moreover, the SVC part can help to balance the source active power. The compensating reactive power passing through SVC part can be expressed as follows:

$$Q_{c1x}=-(Q_{Lx}-Q_{LC}) \quad (6)$$

where the Q_{c1x} are the phase compensating reactive power. The line to line reactive power passing through the SVC part can be expressed as follows:

$$\begin{bmatrix}Q_{c1ab}\\Q_{c1bc}\\Q_{c1ca}\end{bmatrix}=\begin{bmatrix}Q_{c1c}-Q_{c1a}-Q_{c1b}\\Q_{c1a}-Q_{c1b}-Q_{c1c}\\Q_{c1b}-Q_{c1c}-Q_{c1a}\end{bmatrix}=\begin{bmatrix}Q_{La}+Q_{Lb}-Q_{Lc}-Q_{LC}\\Q_{Lb}+Q_{La}-Q_{La}-Q_{LC}\\Q_{Lc}+Q_{La}-Q_{Lb}-Q_{LC}\end{bmatrix} \quad (7)$$

where Q_{LC} is the small and fixed reactive power provided by *LC* part of CGCI, which can be expressed as follows:

$$Q_{LC}=\frac{\bar{V}_x^2}{X_{L_P}-X_{C_P}} \quad (8)$$

where $\bar{V}_x$ is the RMS value of load voltage which can be obtained in real time as $\bar{V}_x=\|v_L\|/\sqrt{3}=\sqrt{v_a^2+v_b^2+v_c^2}/\sqrt{3}$ [22]. X_{Lp} and X_{Cp} are the impedances of L_P and C_P.

The purpose of the SVC part is used to compensate the fundamental reactive and unbalanced power by providing different α_{xy} for each phase. To obtain α_{xy}, the SVC part impedance X_{xy} in real-time is calculated as follows:

$$\begin{bmatrix}X_{ab}\\X_{bc}\\X_{ca}\end{bmatrix}=\begin{bmatrix}\frac{V_{ab}^2}{Q_{c1ab}}\\\frac{V_{bc}^2}{Q_{c1bc}}\\\frac{V_{ca}^2}{Q_{c1ca}}\end{bmatrix}=\begin{bmatrix}\frac{3\cdot\bar{V}_x^2}{Q_{c1ab}}\\\frac{3\cdot\bar{V}_x^2}{Q_{c1bc}}\\\frac{3\cdot\bar{V}_x^2}{Q_{c1ca}}\end{bmatrix}=\begin{bmatrix}\frac{3\cdot\bar{V}_x^2}{Q_{La}+Q_{Lb}-Q_{Lc}-Q_{LC}}\\\frac{3\cdot\bar{V}_x^2}{Q_{Lb}+Q_{La}-Q_{La}-Q_{LC}}\\\frac{3\cdot\bar{V}_x^2}{Q_{Lc}+Q_{La}-Q_{Lb}-Q_{LC}}\end{bmatrix} \quad (9)$$

where V_{xy} and V_x are the RMS values of the line-to-line and phase load voltage, respectively, Q_{Lx} is the phase load reactive power. The V_x and $\mathrm{Q}_{Lx}\approx-\bar{q}_{Lx}/2$ [21]–[24] can be calculated in real-time as follows:

$$\begin{bmatrix}q_{La}\\q_{Lb}\\q_{Lc}\end{bmatrix}=\begin{bmatrix}v_{\mathrm{a}}\cdot i_{L\mathrm{a}}^D-v_{\mathrm{a}}^D\cdot i_{La}\\v_{\mathrm{b}}\cdot i_{Lb}^D-v_b^D\cdot i_{Lb}\\v_{\mathrm{c}}\cdot i_{Lc}^D-v_c^D\cdot i_{Lc}\end{bmatrix} \quad (10)$$

$$V_x=\|v\|/\sqrt{3}=\sqrt{v_a^2+v_b^2+v_c^2}/\sqrt{3} \quad (11)$$

where v_x^D and i_{Lx}^D are obtained by delaying v_x and i_{Lx} by a phase angle of *90º*. q_{Lx} is the phase instantaneous reactive power. Then, $\mathrm{Q}_{Lx}\approx-\bar{q}_{Lx}/2$ is obtained by passing q_{Lx} in (10) through low-pass filters. $\|v\|$ is the norm of the three-phase instantaneous load voltage. After obtaining the X_{xy} through (7)–(11), the α_{xy} is determined by solving the following equation.

$$\begin{bmatrix}X_{ab}(\alpha_{ab})\\X_{bc}(\alpha_{bc})\\X_{ca}(\alpha_{ca})\end{bmatrix}=\begin{bmatrix}\frac{\pi X_{L_{\mathrm{PF}}}X_{C_{\mathrm{PF}}}}{X_{C_{\mathrm{PF}}}[2\pi-2\alpha_{ab}+\sin(2\alpha_{ab})]-\pi X_{L_{\mathrm{PF}}}}+X_{L_c}\\\frac{\pi X_{L_{\mathrm{PF}}}X_{C_{\mathrm{PF}}}}{X_{C_{\mathrm{PF}}}[2\pi-2\alpha_{bc}+\sin(2\alpha_{bc})]-\pi X_{L_{\mathrm{PF}}}}+X_{L_c}\\\frac{\pi X_{L_{\mathrm{PF}}}X_{C_{\mathrm{PF}}}}{X_{C_{\mathrm{PF}}}[2\pi-2\alpha_{ca}+\sin(2\alpha_{ca})]-\pi X_{L_{\mathrm{PF}}}}+X_{L_c}\end{bmatrix} \quad (12)$$

where X_{L_c}, $X_{C_{\mathrm{PF}}}$, and $X_{L_{\mathrm{PF}}}$ are the impedances of the coupling inductor, the SVC capacitor, and inductor, respectively. With the calculated X_{xy} from (7)–(11), the α_{xy} can be determined by solving (12).The details can be found in Section III-C.

B. Operation Principle and Control of CGCI Part

The operation principle and power range of the CGCI part is provided as Section III-B1. The control of CGCI is explained in Section III-B2.

1) Operation Principle and Power Range of CGCI Part: The inverter of CGCI is used to inject active power and reactive power at the fundamental frequency. The injected current from the CGCI and the output voltage of the VSI is given as follows:

$$I_{cx2f} = I_{cx2fp} + j \cdot I_{cx2fq} \tag{13}$$

$$\begin{aligned} V_{\text{inv}xf} &= \overrightarrow{V}_{xf} + X_{LC} \cdot \overrightarrow{I}_{cx2f} \\ &= \overrightarrow{V}_{xf} + X_{LC} \cdot (\overrightarrow{I}_{cx2fp} + j\overrightarrow{I}_{cx2fq}) \end{aligned} \tag{14}$$

where I_{cx2fp} and I_{cx2fq} are the fundamental active and reactive current that injects or absorbs from the grid.

Based on the above (13) and (14), the injected active power and reactive power by CGCI part can be expressed as follows:

$$\begin{aligned} \mathrm{S}_{cx2f} &= \overrightarrow{V}_{xf}\overrightarrow{I}^{*}_{cx2f} = \overrightarrow{V}_{xf} \cdot \left(\frac{\overrightarrow{V}_{\text{inv}xf} - \overrightarrow{V}_{xf}}{jX_{LC}}\right)^{*} \\ &= V_{xf} \cdot \left(\frac{(V_{\text{inv}xf} + jV_{\text{inv}xf}) - V_{xf}}{jX_{LC}}\right)^{*} \\ &= V_{xf} \cdot \left(\frac{V_{\text{inv}xf}}{X_{LC}} + j\frac{V_{\text{inv}xf} - V_{xf}}{X_{LC}}\right) \\ &= \frac{V_{xf}V_{\text{inv}xf}}{X_{LC}} + j \cdot \left(\frac{V_{xf}V_{\text{inv}xf}}{X_{LC}} - \frac{V_{xf}^2}{X_{LC}}\right) \\ &= \quad P_{cx2f} \qquad + \quad jQ_{cx2f} \end{aligned} \tag{15}$$

where * is the conjugate value, $V_{\text{inv}xf}$ and V_{xf} are the fundamental inverter voltage and load voltage. Based on (15), the ratio of $V_{\text{inv}xf}/V_{xf}$ can be expressed as follows:

$$\frac{V_{\text{inv}xf}}{V_{xf}} = \sqrt{\frac{P_{cx2f}^2}{S_{\text{base}}} + \left(\frac{Q_{cx2f}}{S_{\text{base}}} - 1\right)^2} \tag{16}$$

where S_{base} is the base power of CGCI which can be expressed as follows:

$$S_{\text{base}} = \frac{V_{xf}^2}{X_{LC}} \tag{17}$$

where X_{LC} is the fundamental coupling impedance of the CGCI. Based on (16) and (17), the ratio of $V_{\text{inv}xf}/V_{xf}$ in term of P_{cx2f} and Q_{cx2f} can be plotted as Fig. 3.

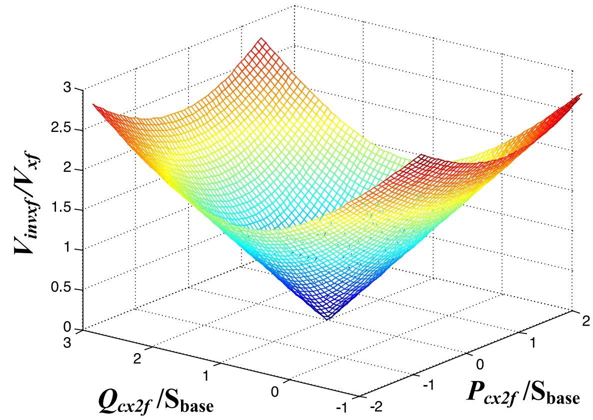

Fig. 3. Ratio of $V_{\text{inv}xf}/V_{xf}$ in term of P_{cxf}/S_{base} and Q_{cx2f}/S_{base}.

In Fig. 3, at the fundamental frequency, the coupling LC of CGCI part is used to compensate fixed amount of reactive power ($Q_{cx2f} = S_{\text{base}}$), and the $V_{\text{inv}xf}$ is used to inject active power.

2) CGCI Part Control: The purpose of the CGCI part is to inject active power $P^*_{cx} = P_{cx2f}$, and compensate the harmonic power and reactive power left by the SVC part. However, to avoid the mistuning problem of the SVC part, the CGCI is controlled to limit the compensating current i_{cx} (instead of inverter current i_{cx2}) to the reference value i^*_{cx}. The i^*_{cx} can be calculated through the well-known instantaneous p–q theory [31] as

$$\begin{bmatrix} i^*_{ca} \\ i^*_{cb} \\ i^*_{cc} \end{bmatrix} = \sqrt{\frac{2}{3}} \cdot \frac{1}{v_\alpha^2 + v_\beta^2} \begin{bmatrix} 1 & 0 \\ -1/2 & \sqrt{3}/2 \\ -1/2 & -\sqrt{3}/2 \end{bmatrix} \cdot \begin{bmatrix} v_\alpha & -v_\beta \\ v_\beta & v_\alpha \end{bmatrix} \begin{bmatrix} \tilde{p}_{\alpha\beta} + 3P^*_{cx} \\ q_{\alpha\beta} \end{bmatrix} \tag{18}$$

where P^*_{cx} is reference phase injected active power, and the total reference active power is $3P^*_{cx}$ for three-phase system, $\tilde{p}_{\alpha\beta}$ is three-phase instantaneous harmonic active power, $q_{\alpha\beta}$ is the three-phase instantaneous reactive power which include harmonic component $\tilde{q}_{\alpha\beta}$ and dc component $\bar{q}_{\alpha\beta}$. As the reference compensating current i^*_{cx} is calculated from $\tilde{p}_{\alpha\beta}$ and $q_{\alpha\beta}$ (included $\tilde{q}_{\alpha\beta}$ component), the three-phase $\tilde{p}_{\alpha\beta}$ and $\tilde{q}_{\alpha\beta}$ fluctuation can be suppressed by limiting the compensating current i_{cx} to track its reference i^*_{cx}. The major part of $\bar{q}_{\alpha\beta}$ is shared by SVC part, while the remaining amount of $\bar{q}_{\alpha\beta}$ for three phase is compensated by LC part of CGCI. The $p_{\alpha\beta}$ and $q_{\alpha\beta}$ can be expressed as follows:

$$\begin{bmatrix} p_{\alpha\beta} \\ q_{\alpha\beta} \end{bmatrix} = \begin{bmatrix} v_\alpha & v_\beta \\ -v_\beta & v_\alpha \end{bmatrix} \cdot \begin{bmatrix} i_\alpha \\ i_\beta \end{bmatrix}. \tag{19}$$

In (18) and (19), the voltages (v_α andv_β) and currents (i_α and i_β) in $\alpha - \beta$ plane are transformed from *a-b-c* frames by

$$\begin{bmatrix} v_\alpha \\ v_\beta \end{bmatrix} = \begin{bmatrix} 1 & -1/2 & -1/2 \\ 0 & \sqrt{3}/2 & -\sqrt{3}/2 \end{bmatrix} \cdot \begin{bmatrix} v_a \\ v_b \\ v_c \end{bmatrix} \tag{20}$$

$$\begin{bmatrix} i_\alpha \\ i_\beta \end{bmatrix} = \begin{bmatrix} 1 & -1/2 & -1/2 \\ 0 & \sqrt{3}/2 & -\sqrt{3}/2 \end{bmatrix} \cdot \begin{bmatrix} i_{La} \\ i_{Lb} \\ i_{Lc} \end{bmatrix} \tag{21}$$

where v_x and i_{Lx} are load voltage and current signals.

C. Overall Control Block of SVC//CGCI

The overall control block of the proposed SVC//CGCI is provided in Fig. 4. According to Fig. 4 and the SVC part control in Section III-A, (10) and (11) are used to calculate the load reactive power q_{Lx} and load voltage V_x. Then, SVC part impedance

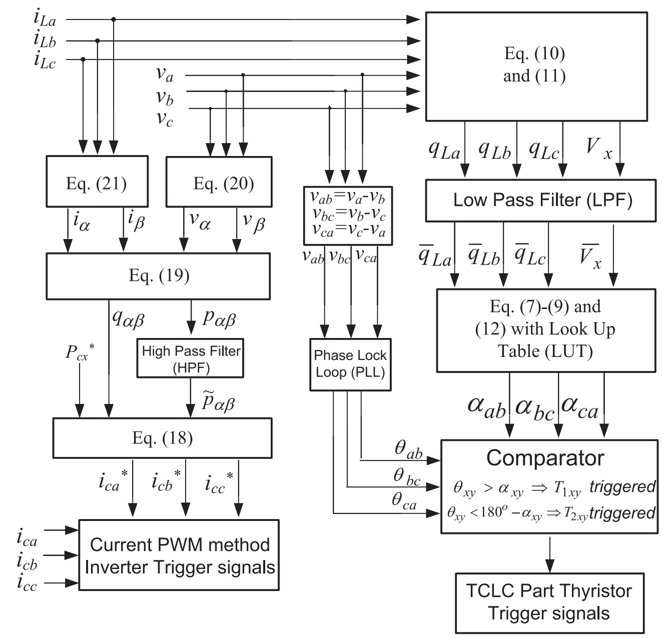

Fig. 4. Overall control block of the proposed SVC//CGCI.

X_{xy} can be obtained from (9) with the help of $\mathrm{Q}_{Lx} \approx -\bar{q}_{Lx}/2$ and reactive power of the coupling LC of CGCI part in (8). After that, by comparing the impedance X_{xy} in (9) and (12), the firing angle α_{xy} can be obtained. As the (12) does not have a closed-form solution, a lookup table has been installed to directly obtain the firing angle α_{xy} with known X_{xy}. By comparing the pre-calculated α_{xy} of the load voltage θ_{xy}, the trigger signals for the thyristor of the SVC can be obtained by using a phase-lock loop.

Based on Fig. 4 and the CGCI part control in Section-B, the load voltage and current (v_x and i_{Lx}) in *a-b-c* frame are transformed to $\alpha{-}\beta$ frame through the (20) and (21). By using the instantaneous *p–q* theory, the instantaneous active power and reactive power in $\alpha{-}\beta$ frame can be calculated through (19).

With the help of the high pass filter and (18), the load reactive power and harmonic active power can be transferred to i^*_{cx}. Through the current hysteresis PWM control method, the trigger signals of the CGCI can be generated by comparing the i_{cx} with i^*_{cx}.

IV. Parameter Design of the Proposed SVC//CGCI

In this section, a parameter design method is discussed and proposed in two parts. In Section IV-A, the parameter design of the C_P and L_p is proposed for the CGCI part. In Section IV-B, the design of L_c, C_{PF}, and L_{PF} is given for the SVC part.

A. Design of C_P and L_P

According to Fig. 3 and (15), the injected active power can be used to determinate the X_{LC}. Based on (15), the X_{LC} is designed as follows:

$$X_{LC} = \frac{V_{xf} V_{\mathrm{inv}xf}}{P_{cx2f(\mathrm{Max})}} \approx \frac{V_{xf} V_{\mathrm{DC}}}{\sqrt{6} \cdot P_{cx2f(\mathrm{Max})}} \tag{22}$$

where $P_{cx2f(\max)}$ is the maximum injected active power can be provided by CGCI, V_{xf} is the load voltage, V_{DC} is designed dc-link voltage. From another perspective, the X_{LC} can be expressed as the impedance of coupling components of CGCI

$$X_{LC} = X_{L_p} - X_{C_P} = \omega \cdot L_p - 1/\omega \cdot C_p \tag{23}$$

where ω is the angular frequency $\omega = 2\pi f$. In (23), the impedance of X_{Cp} is much larger than X_{Lp} ($X_{Cp} >> X_{Lp}$). Therefore, based on (22) and (23), the C_p can be designed as

$$C_p \approx \frac{\sqrt{6} \cdot P_{cxf(\mathrm{Max})}}{2\pi f \cdot V_{xf} V_{\mathrm{DC}}}. \tag{24}$$

The coupling inductor L_P of CGCI is used to reduce the dominant harmonic order n_1 of the loads. By tuning the zero impedance point of $\mathrm{X}_{LC}(n_1\omega) = 0$ in (23) at the dominant harmonic order n_1, the L_p can be expressed as follows:

$$L_p \approx \frac{1}{(2\pi f n_1)^2 \cdot C_p} \tag{25}$$

where n_1 is the dominant harmonic order which is equal to 5th ($n_1 = 5$) for three-phase three-wire system.

B. Design of L_{PF}, C_{PF}, and L_c

The impedance of the SVC part is used to compensate the fundamental reactive power left by the CGCI part. The SVC part impedance can be expressed as follows:

$$\begin{aligned} X_{xy} &= \frac{V_{xy}^2}{Q_{\mathrm{c}1xy}} = \frac{3 \cdot \bar{V}_x^2}{Q_{\mathrm{c}1xy}} = \frac{3 \cdot \bar{V}_x^2}{Q_{Lx} - Q_{LC}} \\ &= \frac{\pi X_{L_{\mathrm{PF}}} X_{C_{\mathrm{PF}}}}{X_{C_{\mathrm{PF}}}[2\pi - 2\alpha_{xy} + \sin(2\alpha_{xy})] - \pi X_{L_{\mathrm{PF}}}} + X_{L_c}. \end{aligned} \tag{26}$$

In (26), X_{Lc}, $X_{C_{\mathrm{PF}}}$, and $X_{L_{\mathrm{PF}}}$ are the fundamental impedances of L_c, C_{PF} and L_{PF}. When $\alpha_x = 180°$ (thyristors are opened for the whole cycle), the SVC part has the maximum capacitive SVC impedance $X_{xy}(\alpha_{xy} = 180°)(< 0)$. At this situation, the SVC part can provide maximum capacitive reactive power $Q_{cx(\mathrm{MaxCap})}$ for maximum inductive loads reactive power compensation $Q_{Lx(\mathrm{MaxInd})}$ $(= -Q_{cx(\mathrm{MaxCap})})$. On the other hand, when $\alpha_{xy} = 90°$ (one of thyristors is closed for whole cycle), the SVC part has the minimum inductive SVC impedance $X_{xy}(\alpha_x = 90°)$. The SVC part can provide maximum inductive reactive power $Q_{cx(\mathrm{MaxInd})}$ for maximum capacitive loads reactive power compensation $Q_{Lx(\mathrm{MaxCap})}$ $(= -Q_{cx(\mathrm{MaxInd})})$. Based on above discussions and (26), the relationship among $Q_{Lx(\mathrm{MaxCap})}$ $Q_{Lx(\mathrm{MaxInd})}$ and coupling SVC impedance can be given by

$$\frac{3 \cdot \bar{V}_x^2}{Q_{Lx(\mathrm{MaxInd})} - Q_{LC}} = X_{xy}(\alpha_{xy} = 180^{\mathrm{o}}) = -\frac{1}{X_{C_{\mathrm{PF}}} - X_{L_c}} \tag{27}$$

$$\begin{aligned} \frac{3 \cdot \bar{V}_x^2}{Q_{Lx(\mathrm{MaxCap})} - Q_{LC}} &= X_{xy}(\alpha_{xy} = 90^{\mathrm{o}}) \\ &= \frac{X_{L_{\mathrm{PF}}} X_{C_{\mathrm{PF}}}}{X_{C_{\mathrm{PF}}} - X_{L_{\mathrm{PF}}}} + X_{L_c}. \end{aligned} \tag{28}$$

TABLE I
PARAMETERS OF IGCI AND SVC//CGCI USED FOR SIMULATION CASE STUDIES

	Parameters	Physical values
System parameters	V_{LL}, f, L_s	191V, 50Hz, 0.2mH
IGCI	L	5mH
SVC//IGCI	$L_c, L_{PF}, C_{PF} L_p$	5mH, 30mH, 160uF, 5mH
SVC//CGCI	$L_c, L_{PF}, C_{PF} L_p, C_P$	5mH, 30mH, 160uF, 5mH, 80uF

Based on (27) and (28), the parallel capacitor C_{PF} and inductor L_{PF} can be designed as follows:

$$C_{\mathrm{PF}} = \frac{Q_{Lx(\mathrm{MaxInd})} - Q_{LC}}{\omega^2 L_c (Q_{Lx(\mathrm{MaxInd})} - Q_{LC}) + 3 \cdot \omega \bar{V}_x^2} \tag{29}$$

$$L_{\mathrm{PF}} = \frac{3\bar{V}_x^2 + \omega L_c (Q_{Lx(\mathrm{MaxCap})} - Q_{LC})}{-\omega (Q_{Lx(\mathrm{MaxCap})} - Q_{LC}) + \omega^3 L_c C_{\mathrm{PF}} (Q_{Lx(\mathrm{MaxCap})} - Q_{LC}) + 3\omega^2 \bar{V}_x^2 C_{\mathrm{PF}}} \tag{30}$$

where Q_{LC} can be found from (8).

The purpose of the L_c design is to mitigate the harmonic currents generated by the thyristors [13]. The thyristors of SVC part can be considered as a pair of bidirectional switches, which would generate low-order harmonic currents when the switches change their states. Through the harmonic currents rejection analysis, the L_c can be expressed as [13]

$$L_c = \frac{1}{(2\pi f n_2)^2 C_{\mathrm{PF}}}, \quad L_c = \frac{1}{(2\pi f n_3)^2 C_{\mathrm{PF}} - 1/L_{\mathrm{PF}}} \tag{31}$$

where the harmonic orders n_2 and n_3 mainly depend on the L_c, L_{PF}, and C_{PF} values. For a three-phase three-wire system, there is no 3nth-order harmonic current and the common harmonic orders are $6n \pm 1 (\geq 5)$ with $n = 1, 2, 3 \ldots$. To avoid the harmonic currents injection by the SVC part, it is suggested to tune n_2 and n_3 to be away from the $6n\pm$ 1st-order and/or close to the 3rd order [13].

V. SIMULATION CASE STUDIES OF THE PROPOSED SVC//CGCI

In this section, the simulation case studies are provided to show the advantages of the proposed SVC//CGCI in comparison with the conventional IGCI and SVC//IGCI. The control scheme of the IGCI is based on the instantaneous reactive power theory, which is valid for sinusoidal or nonsinusoidal (harmonic), balanced or unbalanced three-phase power systems [31]. The parameters of IGCI, SVC//IGCI and the proposed of SVC//CGCI and simulation setups are given in Table I. The selections of dc-link voltage of IGCI and CGCI are provided as follows.

The coupling fundamental impedances for traditional IGCI part and CGCI part are fixed as $X_L (> 0)$ and $X_{Lp} - X_{Cp} (< 0)$. The relationships among the V_x, $V_{\mathrm{inv}xf}$, I_{cx2f}, and the coupling impedance of the traditional IGCI and CGCI can be expressed as follows:

$$V_{\mathrm{inv}xf(\mathrm{IGCI})} = V_x + X_L \cdot I_{cx2f} \tag{32}$$

$$V_{\mathrm{inv}xf(\mathrm{CGCI})} = V_x + (X_{L_p} - X_{C_p}) \cdot I_{cx2f} \tag{33}$$

where $X_L (> 0)$ and $X_{Lp} - X_{Cp} (< 0)$ are the coupling impedance of IGCI and CGCI. I_{cx2f} is the compensating current passing through the coupling impedance. The $X_L (> 0)$ is a small inductive impedance and $X_{Lp} - X_{Cp} (< 0)$ is a large capacitive impedance. In (32), if the I_{cx2f} is the capacitive, the $V_{\mathrm{inv}xf(\mathrm{IGCI})}$ for IGCI is larger than V_x. On the other hand, as (33), the $V_{\mathrm{inv}xf(\mathrm{CGCI})}$ for CGCI is smaller than V_x due to large voltage drop of coupling LC. The fundamental dc-link voltage can be expressed as follows:

$$V_{\mathrm{DC}f} \approx \sqrt{6} \cdot V_{\mathrm{inv}xf} > \sqrt{6} \cdot V_x. \tag{34}$$

In (34), the scale of $\sqrt{6} (= \sqrt{2} \cdot \sqrt{3})$ can be explained by the following two reasons: First, to guarantee the sufficient $V_{\mathrm{DC}f}$, the peak value of fundamental inverter voltage need to be considered $V_{\mathrm{invx}f(p)} > \sqrt{2} \cdot V_{\mathrm{invx}f}$. Second, to transfer the phase voltage $V_{\mathrm{inv}xf}$ to line-to-line dc-link voltage, the scale of $\sqrt{3}$ is required. According to (34), the dc-link voltage of IGCI for the 110 V system $\mathrm{V}_{\mathrm{DC}f} > \sqrt{6} \cdot 110 = 270$ V. The required dc-link voltage of CGCI can be smaller than IGCI. In this section, the dc-link voltage of IGCI and CGCI part are set to be 300 V and 120 V, respectively.

From Fig. 5(a) and Table II, it can be seen that the conventional IGCI can compensate the power factor (PF) to close to unity from original 0.97 and 0.71 for the light harmonic loads and heavy harmonic loads, respectively. Meanwhile, the total harmonic distortion (THD_{isx}) has been improved to lower than 5.4% for light harmonic loads and 4.1% for heavy harmonic loads. The required V_{DC} and I_{cx2} are about 300 V and 7.4 A, respectively.

Based on Fig. 5(b) and Table II, the proposed SVC//CGCI can also compensate the PF to unity for the light harmonic loads (PF = 0.97) and heavy harmonic loads (PF = 0.71), respectively. Meanwhile, the source current THD_{isx} has been improved to lower than 6.1% and 5.1% for light loads with 28.8% and heavy loads with 10.7%, respectively. The required V_{DC} and I_{cx2} are 120 V and 3.2 A, respectively.

During unbalanced loading case, from Fig. 6(a) and Table II, the source reactive power Q_{sx} can be compensated to about zero and the P_{sx} can compensated to be balanced (about 562 W) with $P_{cx}^* = 70$ W. From Fig. 6(a), the PF and THD_{isx} are improved to 0.99 and 15.6% (worst phase) for unbalanced loads after conventional IGCI compensation.

From Fig. 6(b) and Table II, the Q_{sx} can be compensated to about 18 var and the P_{sx} can be balanced to 560 W with $P_{cx}^* = 70$ W. From Fig. 6(b), the PF and THD_{isx} have been compensated to unity and 4.7% (worst phase).

On the other hand, from Fig. 6(c) and Table II, the Q_{sx} can be compensated from 586 var to about 12 var and the P_{sx} can be balanced to 555 W with $P_{cx}^* = 70$ W. From Fig. 6(b), the PF and THD_{isx} have been compensated to unity and 3.5% (worst phase). Compared with IGCI, the proposed SVC//CGCI has better THD_{isx} compensating performance.

Compared with the compensation performance of IGCI ($THD_{isx} > 15.0\%$) in Fig. 6(a), the SVC//IGCI in Fig. 6(b) can obtain better THD_{isx} performance ($\mathrm{THD}_{isx} < 5.0\%$) due to the compensating current sharing by SVC part of the SVC//IGCI.

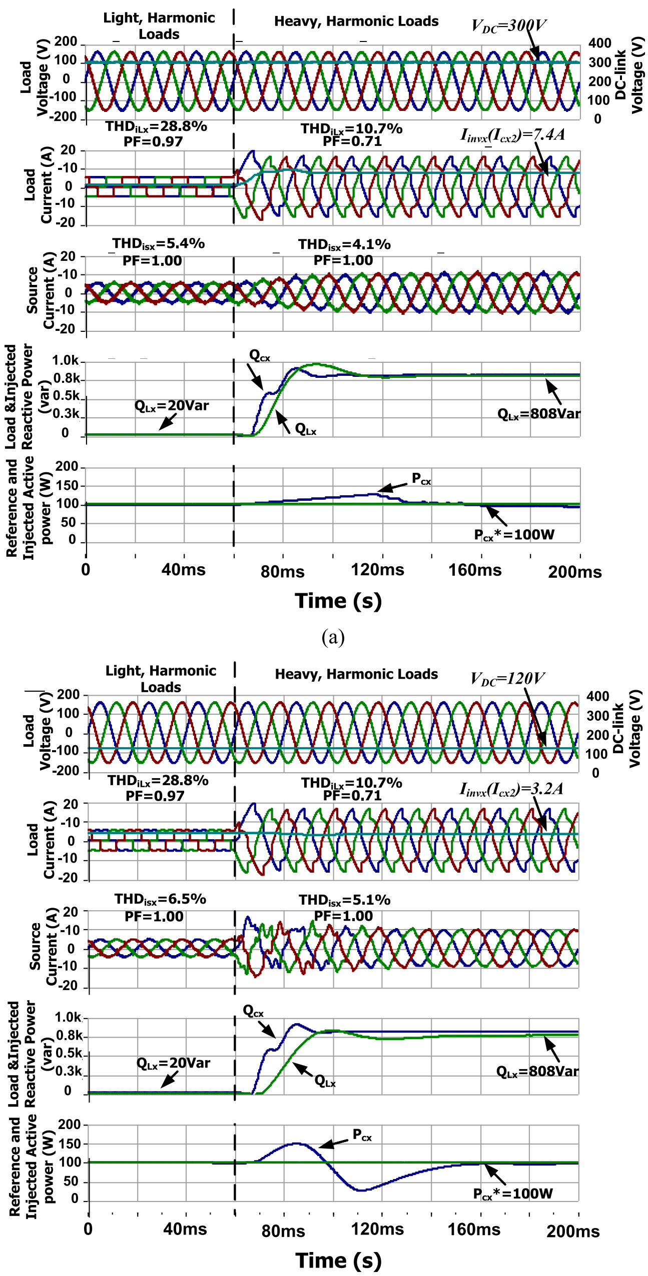

Fig. 5. Waveforms of load voltage, dc-link voltage, load current, inverter current, source current, load and injected reactive power, reference and injected active power for light and heavy harmonic loads compensation by using (a) IGCI and (b) the proposed SVC//CGCI.

Among the three compensators, the SVC//CGCI in Fig. 6(c) obtains the best $\mathrm{THD}_{isx}(< 4.0\%)$ performance. In addition, the required dc-link voltage of SVC//CGCI ($V_{\mathrm{DC}} = 120\,\mathrm{V}$) is smaller than IGCI ($V_{\mathrm{DC}} = 300\,\mathrm{V}$) and SVC//IGCI ($V_{\mathrm{DC}} = 300\,\mathrm{V}$).

Based on Fig. 5, the active inverter capacity of the proposed SVC//CGCI is just 17.3% of IGCI and 38% of SVC//IGCI. The major compensating power capacity of SVC//CGCI is shared by the SVC part and the coupling *LC* of the CGCI. Based on [13]–[15], the costs of IGCI (or active inverter part), PPF and SVC are about \$60/kVA, \$18/kVA, and \$5/kVA, respectively. The cost

TABLE II
SIMULATION RESULTS FOR DIFFERENT LOADS COMPENSATION BEFORE AND AFTER IGCI AND THE PROPOSED SVC//CGCI COMPENSATION

Loads	Compensation		PF	THD_{isx}(%)	P_{sx}(W)	Q_{sx}(var)	i_{invx}(A)	V_{DC}(V)
Light Harmonic Loads	Before comp.		0.97	28.3	442	20	--	--
	IGCI		1.00	5.4	308	9	1.3	300
	SVC//CGCI		1.00	6.1	308	7	3.0	120
Heavy Harmonic, Loads	Before comp.		0.71	10.7	813	808	--	--
	IGCI		1.00	4.1	681	9	7.4	300
	SVC//CGCI		1.00	5.1	680	8	3.6	120
Unbalanced Harmonic Loads	Before comp.	a	0.69	20.2	558	586	--	--
		b	0.84	25.7	546	546		
		c	0.86	18.6	759	349		
	IGCI	a	0.99	15.6	558	12	5.4	300
		b	0.99	3.5	560	14	4.8	
		c	0.99	1.9	567	13	3.4	
	SVC//IGCI	a	1.00	4.4	563	16	3.8	300
		b	1.00	3.8	560	17	3.7	
		c	1.00	4.7	557	18	3.9	
	SVC//CGCI	a	1.00	3.4	558	12	3.8	120
		b	1.00	3.5	550	11	3.5	
		c	1.00	1.9	557	10	3.9	

of SVC//CGCI can be approximately calculated as the sum of cost SVC, PPF, and 17.3% of IGCI. Based on the cost analysis, the cost of the IGCI, SVC//IGCI, and the proposed SVC//CGCI are estimated about 60/kVA, \$68.3/kVA, and \$33.4/kVA (just 56% of IGCI).

VI. EXPERIMENTAL RESULTS

In this section, an 110V-5 kVA experimental prototype of IGCI and SVC//CGCI with the proposed design method is built in laboratory. The photos of the experimental setup of the proposed SVC//CGCI and the different components are shown in Figs. 7 and 8. In Figs. 7 and 8, the digital control system of the SVC//CGCI is digital signal processor (DSP) TMS320F2812, and the sampling frequency of the control system is 25 kHz. The switching devices for the inverter are Mitsubishi insulated gate bipolar transistor (IGBT) intelligent power modules PM300DSA060. The switching devices for the SVC are thyristors SanRex PK110FG160. Moreover, the experimental parameters of the SVC//CGCI are approximately the same as simulation study, which are shown in Table I. During the startup process, the SVC part is turned on first. Until SVC part goes to steady state, the CGCI part is connected to system with the protection of series connected resistors. After the CGCI goes to the steady state, the protect resistors are bypassed.

Fig. 9 illustrates the waveforms of voltage and current by using the conventional IGCI. From Fig. 9(a) and Table III, for the inductive loading, the worst phase PF and THD_{isx} have been improved from original 0.96 and 24.5% to 0.99 and 13.5% after IGCI compensation. From Fig. 9(b) and Table III, for the unbalanced loads compensation, the worst case PF and THD_{isx} have been compensated to 0.98 and 15.4% after IGCI compensation. The dc-link voltage of IGCI is slightly larger than 300 V.

From Figs. 10, 11, and Table III, after SVC//CGCI compensation with $V_{\mathrm{DC}} = 120\,\mathrm{V}$, the worst phase PF has been improved from 0.76 to 0.99. The worst phase THD_{isx} has been kept to about 5.5% (worst phase). Since the proposed SVC//CGCI is connected to a low rating isolation transformer with inductive impedance, the load voltage is increased after reactive power

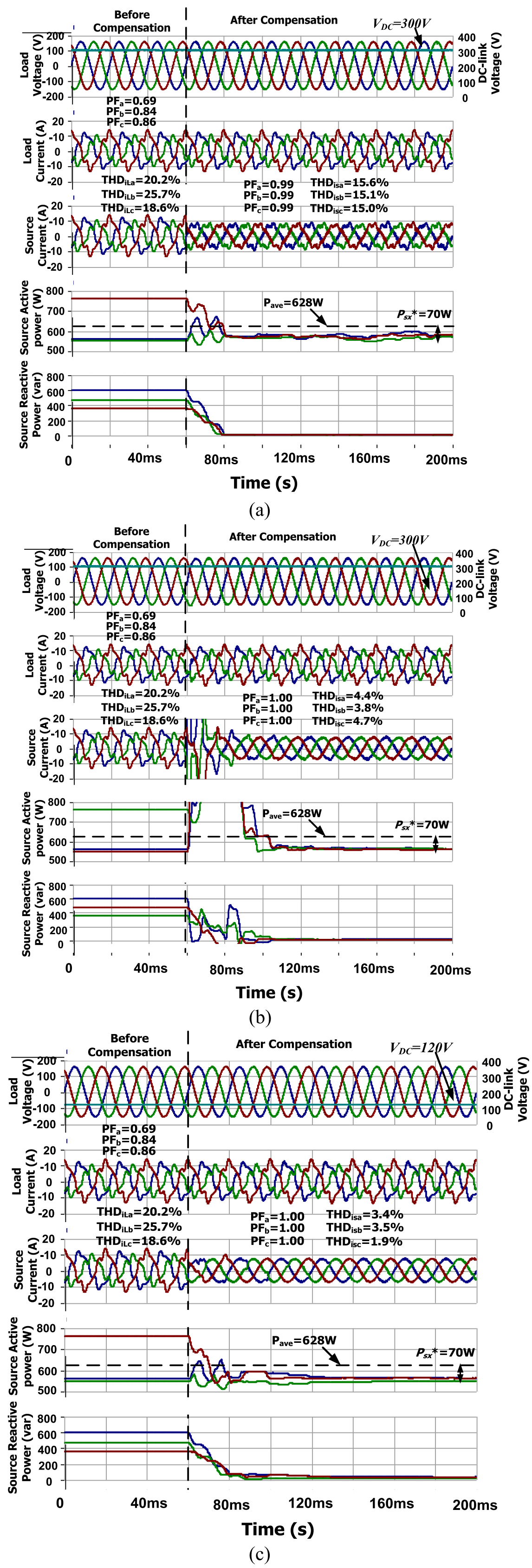

Fig. 6. Waveforms of load voltage, dc-link voltage, load current, source current, source reactive, and active powers for unbalanced harmonic loads compensation by using (a) IGCI, (b)SVC//CGCI, and (c) the proposed SVC//CGCI.

Fig. 7. Experimental setup of the SVC//CGCI experimental prototype.

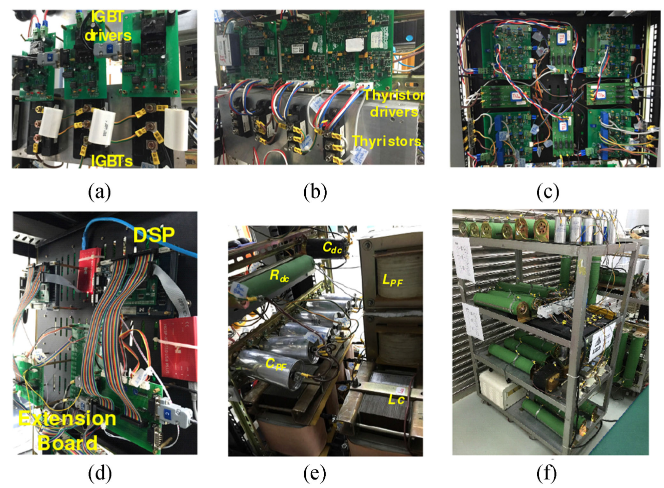

Fig. 8. SVC//CGCI and loading system. (a) IGBTs and their divers. (b) Thyristors and their divers. (c) Transducers with signal conditioning circuits. (d) DSPs and their extension boards. (e) SVC part components, dc capacitor and discharge resistor. (f) Loading system.

compensation. From Fig. 12(a) and (b), after compensation, the load voltage and load active power are slightly increasing due to the inductive impedance of isolation transformer. Compared with load active power (710, 780, and 780 W) in Fig. 12(b), the source active power is reduced to 650 W, 690 W and 680 W after SVC//CGCI compensation as Fig. 12(c) with $P^*_{cx} = 100\,\mathrm{W}$. From Fig. 12(d), it can be seen that reactive power are compensated from 650 var to 80 var for worst phase.

From Figs. 13, 14, and Table III, after SVC//CGCI compensation with $V_{\mathrm{DC}} = 120\,\mathrm{V}$, the PF has been compensated from 0.69, 0.76, and 0.83 to 0.99 for three phases under unbalanced loads compensation. The source current THD$_{isx}$ has been improved to 9.8% for the worst phase. In Fig. 15, it can be seen that the load voltage and source current are in phase with each other after compensation even under unbalanced loads. From Fig. 16(b) and (c), after SVC//CGCI compensation, the source active power of three phases have been balanced to 620, 620, and 600 W. Compared with the load active power (660, 650, and 840 W), the total source active power is reduced due to active power injection by the CGCI part with $P^*_{cx} = 70\,\mathrm{W}$. Meanwhile,

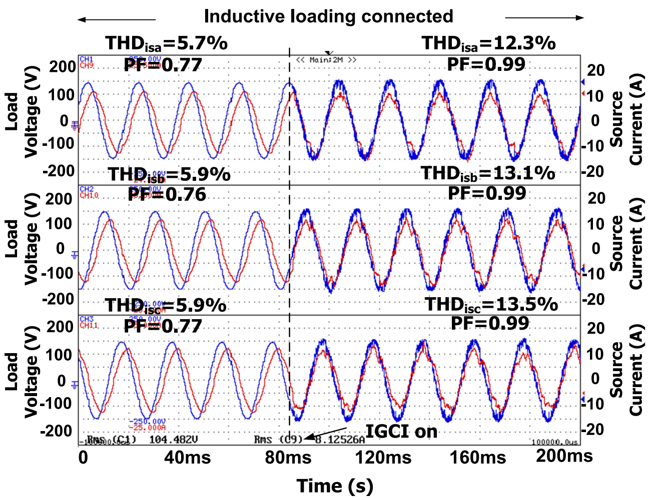

(a)

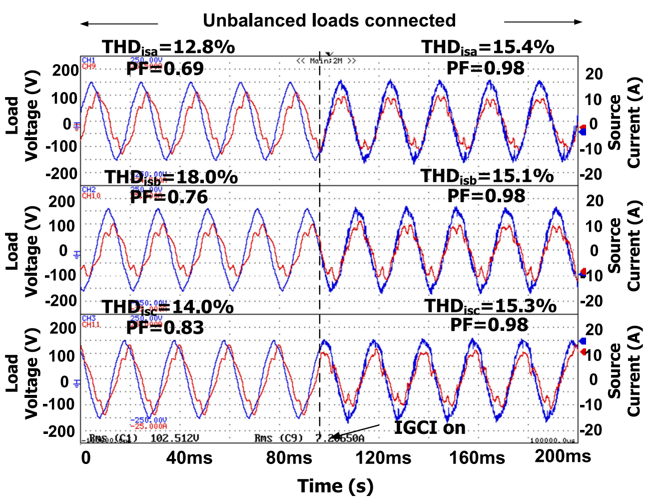

(b)

Fig. 9. Waveforms of v_x and i_{sx} by using IGCI for reactive power and harmonic compensation. (a) During inductive loads. (b) During unbalanced loads.

TABLE III
EXPERIMENTAL RESULTS FOR DIFFERENT LOADS BEFORE AND AFTER SVC//CGCI COMPENSATION

			Q_{sx}(var)	P_{sx}(W)	PF	THD_{isx}(%)	V_{DC}(V)
Inductive loads	Before Comp.	A	650	700	0.77	5.7	--
		B	650	740	0.76	5.9	
		C	650	740	0.77	5.9	
	IGCI	A	70	690	0.99	12.3	320
		B	80	700	0.99	13.1	
		C	70	700	0.99	13.5	
	SVC//CGCI	A	60	650	0.99	5.3	120
		B	50	690	0.99	5.4	
		C	80	680	0.99	5.5	
Unbalanced loads	Before Comp.	A	600	590	0.69	12.8	--
		B	480	560	0.76	18.0	
		C	520	780	0.83	14.0	
	IGCI	A	70	640	0.98	15.4	320
		B	90	630	0.98	15.3	
		C	80	630	0.98	15.4	
	SVC//CGCI	A	10	620	0.99	8.4	120
		B	80	620	0.99	6.9	
		C	20	600	0.99	9.8	

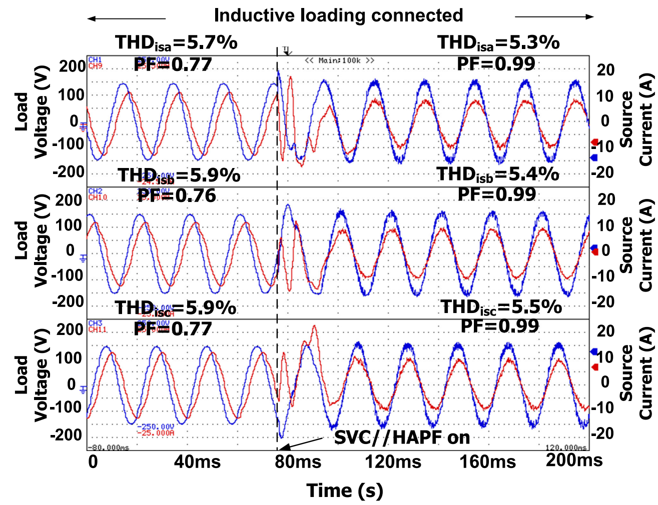

Fig. 10. Waveforms of v_x and i_{sx} by using SVC//CGCI for active power injection and nonactive power compensation under inductive loads.

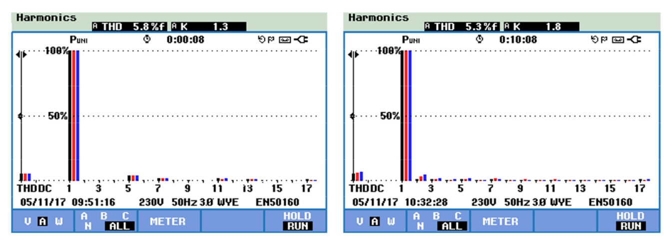

(a) (b)

Fig. 11. i_{sx} harmonic spectrums of SVC//CGCI for harmonic loads compensation. (a) Before compensation. (b) After compensation.

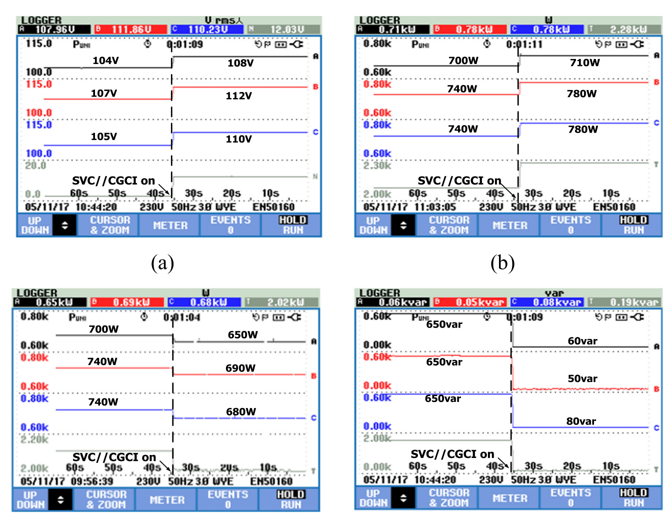

(a) (b)

(c) (d)

Fig. 12. Waveforms before and after SVC//CGCI compensation for harmonic loads compensation. (a) Load voltage. (b) Load active power. (c) Source active power. (d) Source reactive power.

the source reactive power has been compensated from 600, 480, and 520 var to 10, 80, and 20 var, as shown in Fig. 16(d).

Compared the experiments results of the IGCI with the proposed SVC//CGCI, the SVC//CGCI obtains better compensation performances (PF and THD_{isx}) with lower dc-link voltage.

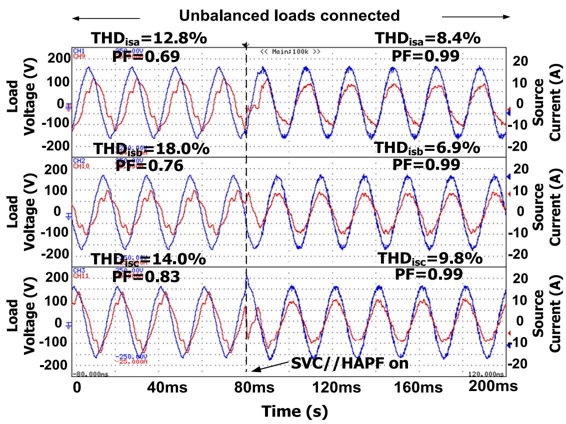

Fig. 13. Waveforms of v_x and i_{sx} by using SVC//CGCI for active power injection and nonactive power compensation under unbalanced loads.

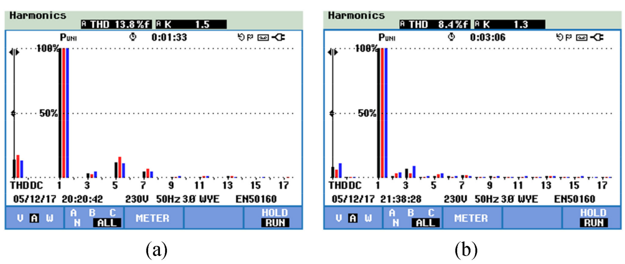

Fig. 14. i_{sx} harmonic spectrums of SVC//CGCI for unbalanced harmonic loads compensation. (a) Before compensation. (b) After compensation.

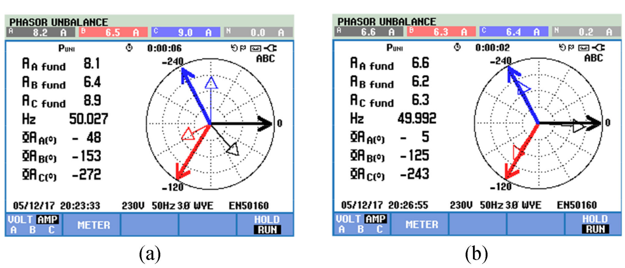

Fig. 15. Vector diagram of SVC//CGCI for unbalanced loads. (a) Before compensation. (b) After compensation.

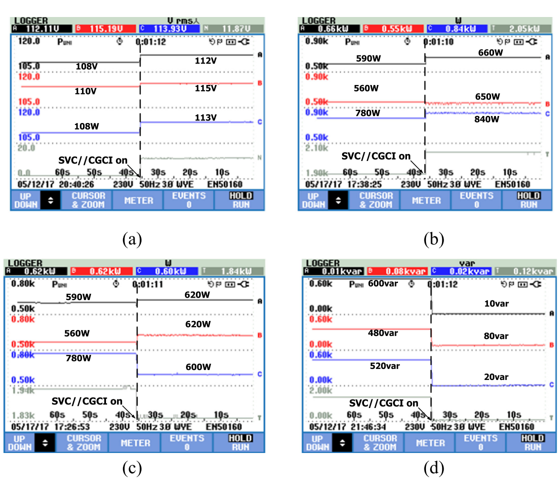

Fig. 16. Waveforms before and after SVC//CGCI compensation for unbalanced loads. (a) Load voltage. (b) Load active power. (c) Source active power. (d) Source reactive power.

VII. Conclusion

In this paper, a new structure of SVC in parallel with CGCI (SVC//CGCI) in a three-phase power system was proposed and discussed as a cost-effective solution for active power injection and nonactive power (harmonic, reactive, and unbalanced power) compensation. The SVC part was used to dynamically compensate the reactive power and balance the source active power. The CGCI was used to compensate harmonic power and provide a fixed amount of reactive power (coupling LC). Finally, representative simulation and experimental results are provided to show that the SVC//CGCI has the great promise for wide operation range with both low voltage and current rating of active inverter.

References

[1] E. Santacana, G. Rackliffe, L. Tang, and X. Feng, "Getting smart," *IEEE Power Energy Mag.*, vol. 8, no. 2, pp. 41–48, Apr. 2010.

[2] Z. Shuai *et al.*, "Microgrid stability: Classification and a review," *Renew. Sustain. Energy Rev.*, vol. 58, pp. 167–179, May 2016.

[3] H. Han, X. Hou, J. Yang, J. Wu, M. Su, and J. M. Guerrero, "Review of power sharing control strategies for islanding operation of ac microgrids," *IEEE Trans. Smart. Grid*, vol. 7, no. 1, pp. 200–215, Jan. 2016.

[4] B. Wang, L. Xian, V. R. K. Kanamarlapudi, K. J. Tseng, A. Ukil, and H. B. Gooi, "A digital method of power-sharing and cross-regulation suppression for single-inductor multiple-input multiple-output dc–dcconverter," *IEEE Trans. Ind. Electron.*, vol. 64, no. 4, pp. 2836–2847, Apr. 2017.

[5] Z. Shuai, Y. Hu, Y. Peng, C. Tu, and Z. J. Shen, "Dynamic stability analysis of synchronverter-dominated microgrid based on bifurcation theory," *IEEE Trans. Ind. Electron.*, vol. 64, no. 9, pp. 7467–7477, Sep. 2017.

[6] Z. Shuai, W. Huang, C. Shen, J. Ge, and Z. J. Shen, "Characteristics and restraining method of fast transient inrush fault currents in synchronverters," *IEEE Trans. Ind. Electron.*, vol. 64, no. 9, pp. 7487–7497, Sep. 2017.

[7] H. Komurcugil, N. Altin, S. Ozdemir, and I. Sefa, "Lyapunov-function and proportional-resonant-based control strategy for single-phase grid-connected VSI with LCL filter," *IEEE Trans. Ind. Electron.*, vol. 63, no. 5, pp. 2838–2849, May 2016.

[8] Q. C. Zhong, Y. Wang, and B. Ren, "UDE-based robust droop control of inverters in parallel operation," *IEEE Trans. Ind. Electron.*, vol. 64, no. 9, pp. 7552–7562, Sep. 2017.

[9] S. Dasgupta, S. N. Mohan, S. K. Sahoo, and S. K. Panda, "Application of four-switch-based three-phase grid-connected inverter to connect renewable energy source to a generalized unbalanced microgrid system," *IEEE Trans. Ind. Electron.*, vol. 60, no. 3, pp. 1204–1215, Mar. 2013.

[10] A. Shayestehfard, S. Mekhilef, and H. Mokhlis, "IZDPWM-based feedforward controller for grid-connected inverters under unbalanced and distorted conditions," *IEEE Trans. Ind. Electron.*, vol. 64, no. 1, pp. 14–21, Jan. 2017.

[11] M. Singh and A. Chandra, "Real-time implementation of and is control for renewable interfacing inverter in 3p4w distribution network," *IEEE Trans. Ind. Electron.*, vol. 60, no. 1, pp. 121–128, Jan. 2013.

[12] R. Chilipi, N. Al sayari, K. H. Al Hosani, and A. R. Beig, "Adaptive notch filter based multipurpose control scheme for grid-interfaced three-phase four-wire DG inverter," *IEEE Trans. Ind. Appl.*, vol. 53, no. 4, pp. 4015–4027, Jul./Aug. 2017.

[13] L. Wang, C. S. Lam, and M. C. Wong, "Design of A thyristor controlled LC compensator for dynamic reactive power compensation in smart grid," *IEEE Trans. Smart. Grid*, vol. 8, no. 1, pp. 409–417, Jan. 2017.

[14] K. W. Lao, M. C. Wong, N. Dai, C. K. Wong, and C. S. Lam, "A systematic approach to hybrid railway power conditioner design with harmonic compensation for high-speed railway," *IEEE Trans. Ind. Electron.*, vol. 62, no. 2, pp. 930–942, Feb. 2015.

[15] K. W. Lao, N. Dai, W. G. Liu, and M. C. Wong, "Hybrid power quality compensator with minimum dc operation voltage design for high-speed traction power systems," *IEEE Trans. Power. Electron.*, vol. 28, no. 4, pp. 2024–2036, Apr. 2013.

[16] A. Varschavsky, J. Dixon, M. Rotella, and L. Moran, "Cascaded nine-level inverter for hybrid-series active power filter, using industrial controller," *IEEE Trans. Ind. Electron.*, vol. 57, no. 8, pp. 2761–2767, Aug. 2010.

[17] S. P. Litran and P. Salmeron, "Reference voltage optimization of a hybrid filter for nonlinear load reference," *IEEE Trans. Ind. Electron.*, vol. 61, no. 6, pp. 2648–2654, Jun. 2014.
[18] J. Dixon, Y. del Valle, M. Orchard, M. Ortuzar, L. Moran, and C. Maffrand, "A full compensating system for general loads, based on a combination of thyristor binary compensator, and a PWM-IGBT active power filter," *IEEE Trans. Ind. Electron.*, vol. 50, no. 5, pp. 982–989, Oct. 2003.
[19] "A matter of FACTS, Deliver more, high quality power," ABB Company, Västerås, Sweden, 2016.
[20] L. Wang, C. S. Lam, and M. C. Wong, "Selective compensation of distortion, unbalanced and reactive power of a thyristor controlled LC-coupling hybrid active power filter (SVC-HAPF)," *IEEE Trans. Power Electron.*, vol. 32, no. 12, pp. 9065–9077, Dec. 2017.
[21] L. Wang, C. S. Lam, and M. C. Wong, "A hybrid STATCOM with wide compensation range and low dc-link voltage," *IEEE Trans. Ind. Electron.*, vol. 63, no. 6, pp. 3333–3343, Jun. 2016.
[22] L. Wang, C. S. Lam, and M. C. Wong, "Modeling and parameter design of thyristor controlled LC-coupled hybrid active power filter (SVC-HAPF) for unbalanced compensation," *IEEE Trans. Ind. Electron.*, vol. 64, no. 3, pp. 1827–1840, Mar. 2017.
[23] C. S. Lam, L. Wang, S. I. Ho, and M. C. Wong, "Adaptive thyristor controlled LC-hybrid active power filter for reactive power and current harmonics compensation with switching loss reduction," *IEEE Trans. Power Electron.*, vol. 32, no. 10, pp. 7577–7590, Oct. 2017.
[24] L. Wang, C. S. Lam, and M. C. Wong, "Unbalanced control strategy for a thyristor controlled LC-coupling hybrid active power filter (SVC-HAPF) in three-phase three-wire systems," *IEEE Trans. Power Electron.*, vol. 32, no. 2, pp. 1056–1069, Feb. 2017.
[25] A. Luo, S. Peng, C. Wu, J. Wu, and Z. Shuai, "Power electronic hybrid system for load balancing compensation and frequency-selective harmonic suppression," *IEEE Trans. Ind. Electron.*, vol. 59, no. 2, pp. 723–732, Feb. 2012.
[26] F. R. Quintela, J. M. G. Arevalo, and R. C. Redondo, "Power analysis of static var compensators," *Elect. Power Syst. Res.*, vol. 30, no. 6, pp. 376–382, 2008.
[27] L. Gyugyi, R. A. Otto, and T. H. Putman, "Principles and applications of static thyristor-controlled shunt compensators," *IEEE Trans. Power App. Syst.*, vol. PAS-97, no. 5, pp. 1935–1945, Sep./Oct. 1978.
[28] T. J. Dionise, "Assessing the performance of a static var compensator for an electric arc furnace," *IEEE Trans. Ind. Appl.*, vol. 50, no. 3, pp. 1619–1629, Jun. 2014.
[29] T. Ye, N. Dai, C. S. Lam, M. C. Wong, and J. M. Guerrero, "Analysis, design, and implementation of a quasi-proportional-resonant controller for a multifunctional capacitive-coupling grid-connected inverter," *IEEE Trans. Ind. Appl.*, vol. 52, no. 5, pp. 4269–4280, Sep.-Oct. 2016.
[30] N. Y. Dai, W. C. Zhang, M. C. Wong, J. M. Guerrero, and C. S. Lam, "Analysis, control and experimental verification of a single-phase capacitive-coupling grid-connected inverter," *IET Power Electron.*, vol. 8, pp. 770–782, 2015.
[31] H. Akagi, Y. Kanazawa, and A. Nabae, "Instantaneous reactive power compensators comprising switching devices without energy storage components," *IEEE Trans. Ind. Appl.*, vol. IA–20, no. 3, pp. 625–630, May 1984.

Lei Wang (M'18) received the B.Sc. degree in electrical and electronics engineering and the Ph.D. degree in electrical and computer engineering from University of Macau (UM), Macao, China, in 2011 and 2017, respectively, and the M.Sc. degree in electronics engineering from Hong Kong University of Science and Technology, Hong Kong, in 2012.

He is currently a Postdoctoral Fellow in the Power Electronics Laboratory, UM. His research interests included power electronics, power quality and distribution flexible ac transmission system, power quality compensation, and renewable energy.

Dr. Wang was the recipient of the Champion Award in the "Schneider Electric Energy Efficiency Cup", Hong Kong, 2011.

Chi-Seng Lam (S'04–M'12–SM'16) received the B.Sc., M.Sc., and Ph.D. degrees in electrical and electronics engineering from the University of Macau (UM), Macau, China, in 2003, 2006, and 2012, respectively.

From 2006 to 2009, he was an Electrical and Mechanical Engineer with UM. In 2009, he simultaneously worked as a Laboratory Technician and started to pursue the Ph.D. degree, and completed the Ph.D. within three years. In 2013, he was a Postdoctoral Fellow with The Hong Kong Polytechnic University, Hong Kong. He is currently an Assistant Professor with the State Key Laboratory of Analog and Mixed-Signal VLSI, UM. He has coauthored two Springer books, six patents (China and USA), and more than 70 technical journals and conference papers. His research interests include integrated controllers, power management integrated circuits, power quality compensators, smart grid technology, and renewable energy.

Dr. Lam is a Vice-Chair of the IEEE Macau Section and a Chair of IEEE CAS Macau Chapter. He was the recipient of IEEE PES Chapter Outstanding Engineer Award in 2016, the Macao Science and Technology Invention Award (Third-Class) and R&D Award for Postgraduates (Ph.D.) in 2014 and 2012, respectively, and the RIUPEEEC Merit Paper Award in 2005.

Man-Chung Wong (SM'06) received the B. Sc. and M. Sc. degrees in electrical and electronics engineering from the University of Macau (UM), Macau, China, in 1993 and 1997, respectively, and the Ph.D. degree in electrical engineering from Tsinghua University, Beijing, China, in 2003.

He is currently an Associate Professor with the Department of Electrical and Computer Engineering, UM. He has coauthored two Springer books, eight patents (China and USA), and more than 100 journal and conference papers. His research interests include power electronics converter, pulsewidth modulation, active power filters, and hybrid active power filters.

Dr. Wong was the recipient of Macao Young Scientific Award from Macau International Research Institute in 2000, Young Scholar Award of UM in 2001, Second Prize for Tsinghua University Excellent Ph.D. Thesis Award in 2003 and Macao Science and Technology Invention Award (Third-Class) in 2012 and 2014, respectively. He is currently the North Representative of IEEE Region 10 Power and Energy Society and Chair of IEEE Macau PES/PELS Joint Chapter. He was the Chair of IEEE Macau Section during 2014–2015. He was a visiting fellow in Cambridge University, U.K. in 2014.